Organic Glasses with Exceptional Thermodynamic and Kinetic Stability

Stephen F. Swallen *et al.*

Science **315**, 353 (2007);
DOI: 10.1126/science.1135795

Science (print ISSN 0036-8075; online ISSN 1095-9203) is published weekly, except the last week in December, by the American Association for the Advancement of Science, 1200 New York Avenue NW, Washington, DC 20005.

cutoff (*18*). The cross-sectional area of the simulation cell is 15.3 × 13.3 Å. Along the (001) direction, two sizes were selected: 160 and 320 Å. Periodic boundary conditions were used for all directions. Newton's equations of motions were solved by the fifth-order predictor corrector algorithm (*18*) with an MD time step, $\Delta t = 1.8 \times 10^{-15}$ s.

The simulation cell for the thermal transport measurement is depicted in Fig. 4. To calculate the thermal conductivity, the we first equilibrated the structure at $T = 300$ K for 100,000 MD time steps. Next, the global thermostat was turned off and thermal energy was added to one WSe_2 sheet and removed from a second sheet, which was located at a distance from the first sheet equal to one-half of the size of the simulation cell along the (001) direction (*19*, *20*). Atomic velocities were scaled such that heat was added or subtracted at a constant rate, 10^{-6} eV per MD time step (*21*). We monitored the temperature profile by averaging the kinetic energy of atoms in each WSe_2 sheet. Because of the small energy barrier for shearing of the WSe_2 structure and the small cross-sectional area of the simulation cell, our model structures exhibited thermally excited local shearing events leading to disorder in the stacking of the WSe_2 sheets (Fig. 4).

After 5 to 20 million MD steps (depending on the system size), a steady-state temperature distribution was established (Fig. 4). The temperature gradient, and thus the thermal conductivity, of 16- and 32-nm-long simulation cells were essentially the same within the statistical standard deviation of 10%, $\Lambda = 0.06$ W m^{-1} K^{-1}. Given the approximate form of the potentials used in our computational work, the agreement between the measured and calculated thermal conductivities was better than we expected. Nevertheless, the low thermal conductivity of the model structure suggests that the ultralow thermal conductivity in disordered, layered crystals is a general phenomenon and not restricted to WSe_2.

Our WSe_2 films are poor electrical conductors in the cross-plane direction; however, if semiconductors with similar structural features and good electrical mobility can be identified, disordered layered crystals may offer a promising route to improved materials for thermoelectric energy conversion.

References and Notes

1. D. G. Cahill, S. K. Watson, R. O. Pohl, *Phys. Rev. B* **46**, 6131 (1992).
2. P. B. Allen, J. L. Feldman, *Phys. Rev. B* **48**, 12581 (1993).
3. R. M. Costescu, D. G. Cahill, F. H. Fabreguette, Z. A. Sechrist, S. M. George, *Science* **303**, 989 (2004).
4. Y. S. Ju, M.-T. Hung, M. J. Carey, M.-C. Cyrille, J. R. Childress, *Appl. Phys. Lett.* **86**, 203113 (2005).
5. S. Moss, M. Noh, K. H. Jeong, D. H. Kim, D. C. Johnson, *Chem. Mater.* **8**, 1853 (1996).
6. Materials and methods are available as supporting material on *Science* Online.
7. W. J. Schutte, J. L. De Boer, F. Jellinek, *J. Solid State Chem.* **70**, 207 (1987).
8. J. A. Wilson, A. D. Yoffe, *Adv. Phys.* **18**, 193 (1969).
9. C. A. Paddock, G. L. Eesley, *J. Appl. Phys.* **60**, 285 (1986).
10. R. J. Stoner, H. J. Maris, *Phys. Rev. B* **48**, 16373 (1993).
11. D. G. Cahill, *Rev. Sci. Instrum.* **75**, 5119 (2004).
12. D. G. Cahill, F. Watanabe, *Phys. Rev. B* **70**, 235322 (2004).
13. K. E. O'Hara, X. Hu, D. G. Cahill, *J. Appl. Phys.* **90**, 4852 (2001).
14. H. T. Grahn, H. J. Maris, J. Tauc, *IEEE J. Quantum Electron.* **25**, 2562 (1989).
15. H.-N. Lin, R. J. Stoner, H. J. Maris, J. Tauc, *J. Appl. Phys.* **69**, 3816 (1991).
16. D. E. Moncton, J. D. Axe, F. J. DiSalvo, *Phys. Rev. B* **16**, 801 (1977).
17. P. A. Medwick, R. O. Pohl, *J. Solid State Chem.* **133**, 44 (1997).
18. M. P. Allen, D. J. Tildesley, *Computer Simulation of Liquids* (Oxford Univ. Press, New York, 1987).
19. A. Maiti, G. D. Mahan, S. T. Pantelides, *Solid State Commun.* **102**, 517 (1997).
20. P. K. Schelling, S. R. Phillpot, P. Keblinski, *Phys. Rev. B* **65**, 144306 (2002).
21. P. Jund, R. Jullien, *Phys. Rev. B* **59**, 13707 (1999).

22. Supported by Office of Naval Research grant nos. N00014-05-1-0250 and N00014-96-0407. Research for this work was performed in the Laser and Spectroscopy Facility and the Center for Microanalysis of Materials of the Frederick Seitz Materials Research Laboratory, University of Illinois, which is partially supported by the U.S. Department of Energy under grant DEFG02-91-ER45439. Use of the Advanced Photon Source was supported by the U.S. Department of Energy, Office of Science, Office of Basic Energy Sciences, under contract no. W-31-109-ENG-38.

Supporting Online Material

www.sciencemag.org/cgi/content/full/1136494/DC1
Materials and Methods
Figs. S1 to S5
References

19 October 2006; accepted 4 December 2006
Published online 14 December 2006;
10.1126/science.1136494
Include this information when citing this paper.

Organic Glasses with Exceptional Thermodynamic and Kinetic Stability

Stephen F. Swallen,[1] Kenneth L. Kearns,[1] Marie K. Mapes,[1] Yong Seol Kim,[1] Robert J. McMahon,[1] M. D. Ediger,[1]* Tian Wu,[2] Lian Yu,[2] Sushil Satija[3]

Vapor deposition has been used to create glassy materials with extraordinary thermodynamic and kinetic stability and high density. For glasses prepared from indomethacin or 1,3-bis-(1-naphthyl)-5-(2-naphthyl)benzene, stability is optimized when deposition occurs on substrates at a temperature of 50 K below the conventional glass transition temperature. We attribute the substantial improvement in thermodynamic and kinetic properties to enhanced mobility within a few nanometers of the glass surface during deposition. This technique provides an efficient means of producing glassy materials that are low on the energy landscape and could affect technologies such as amorphous pharmaceuticals.

Glassy materials combine the disordered structure of a liquid with the mechanical properties of a solid. Amorphous systems can be described in terms of a potential energy landscape, with thermodynamics and kinetics controlled by the minima and barriers on the landscape, respectively (*1*–*3*). Many important issues could be addressed if liquids or glasses with very low energies could be created (*2*, *4*–*6*). For example, it might be possible to definitively understand the Kauzmann entropy crisis, an area of intense recent interest (*1*, *7*–*11*). Kauzmann observed that if the entropy of many supercooled liquids is extrapolated to low temperature, the amorphous state is predicted to have a lower entropy than that of the highly ordered crystal well above absolute zero (*5*, *6*).

Glasses are usually prepared by cooling a liquid, but accessing low energy states by this route is impractically slow (*4*, *12*). If a liquid avoids crystallization as it is cooled, molecular motion eventually becomes too slow to allow the molecules to find equilibrium configurations. This transition to a nonequilibrium state defines the glass transition temperature T_g. Glasses are "stuck" in local minima on the potential energy landscape (*2*, *3*). Because glasses are thermodynamically unstable, lower energies in the landscape are eventually achieved through molecular rearrangements. However, this process is so slow that it is generally impossible to reach states deep in the landscape by this route.

We have discovered that vapor deposition can bypass these kinetic restrictions and produce glassy materials that have extraordinary energetic and kinetic stability and unusually high densities. We demonstrate this for two molecular glass formers: 1,3-bis-(1-naphthyl)-5-(2-naphthyl)benzene (TNB) (T_g = 347 K) and indomethacin (IMC) (T_g = 315 K). For these systems, the most stable glasses are obtained when vapor is deposited onto a substrate controlled near T_g – 50 K. We argue that surface mobility during the deposition process is the mechanism of stable glass formation.

Differential scanning calorimetry (DSC) was used to examine the kinetics and thermodynamics of vapor-deposited samples created by heating crystalline TNB or IMC in a vacuum. Figure 1A shows DSC data for TNB vapor-deposited (blue) onto a substrate held at 296 K.

[1]Department of Chemistry, University of Wisconsin–Madison, Madison, WI 53706, USA. [2]School of Pharmacy, University of Wisconsin–Madison, Madison, WI 53705, USA. [3]Center for Neutron Research, National Institute of Standards and Technology, Gaithersburg, MD 20899, USA.

*To whom correspondence should be addressed. E-mail: ediger@chem.wisc.edu

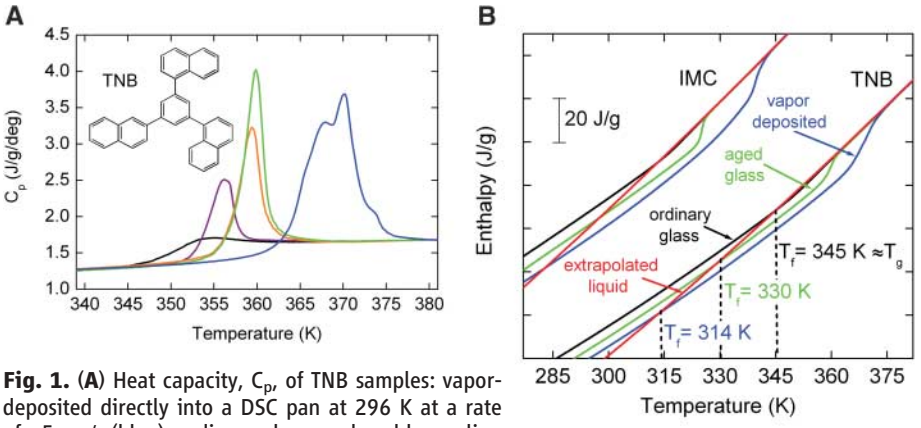

Fig. 1. (**A**) Heat capacity, C_p, of TNB samples: vapor-deposited directly into a DSC pan at 296 K at a rate of ~5 nm/s (blue); ordinary glass produced by cooling the liquid at 40 K/min (black); ordinary glass annealed at 296 K for 174 days (violet), 328 K for 9 days (gold), and 328 K for 15 days (green). (Inset) Structure of TNB. (**B**) Enthalpy of TNB and IMC samples. Heat capacities of the samples shown in (A) are integrated to obtain the curves shown for TNB. Similar experimental conditions were used for IMC (*15*).

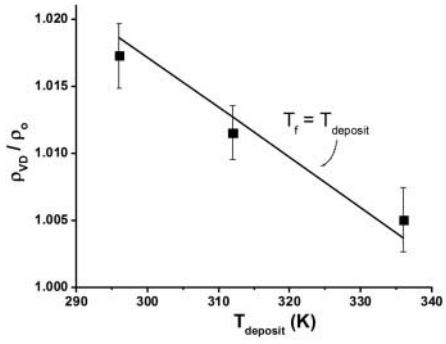

Fig. 2. Density of vapor-deposited TNB films (ρ_{VD}) normalized to the density of the ordinary glass (ρ_o), with both measured at room temperature. Experimental density ratios (filled squares) were calculated from x-ray reflectivity measurements on 100- to 300-nm films by measuring film thickness before and after annealing above T_g (*15*). The solid line indicates the expected density if the samples were prepared in thermal equilibrium with $T_f = T_{deposit}$.

This scan was continued beyond the melting point, after which the sample was cooled into the glass and then scanned again to yield the black curve. This latter curve represents the behavior of an ordinary glass of TNB, with T_g = 347 K, as defined by the onset temperature; it is consistent with previously reported results for TNB (*13*–*15*).

Remarkably, the vapor-deposited sample has a substantially higher onset temperature of 363 K. This result indicates that the vapor-deposited material is kinetically much more stable, because higher temperatures are required to dislodge the molecules from their glassy configurations. For comparison, we isothermally annealed the ordinary glass for 6 months at 296 K and up to 15 days at 328 K (equilibrium was reached at 328 K). Vapor-deposited samples created in only a few hours have much greater kinetic stability than ordinary glasses aged for many days or months below T_g.

To quantify the thermodynamic stability of the vapor-deposited materials, we calculate the fictive temperature (T_f), as defined below. Lower T_f values indicate a lower position in the energy landscape. The enthalpy for TNB and IMC samples, obtained by integrating the heat capacity C_p, is plotted in Fig. 1B. The intersection between these data and the extrapolated supercooled liquid enthalpy (red curve) defines T_f for each sample. For both TNB and IMC, samples prepared by vapor deposition have considerably lower enthalpies and T_f values. On the basis of aging experiments on TNB, we estimate that it would require at least 40 years of annealing an ordinary glass to match T_f for the vapor-deposited sample shown in Fig. 1 (*12*). The similarity of the results for TNB and IMC suggests that vapor deposition can generally produce highly stable glasses.

The thermodynamic stability of these films can also be quantified in comparison with the Kauzmann temperature (T_K), the temperature at which the extrapolated entropy of the supercooled liquid equals that of the crystal (*4*, *5*). We define a figure of merit:

$$\theta_K = \frac{T_g - T_f}{T_g - T_K} \quad (1)$$

For fragile glassformers such as TNB and IMC, θ_K is a measure of position on the energy landscape, with a value of 1 ($T_f = T_K$) indicating the lowest possible position on the landscape. For TNB, Magill estimated T_K = 270 K (*14*). Vapor deposition of TNB at T_g – 50 K created films with θ_K = 0.43; by this measure, we have proceeded 43% toward the bottom of the energy landscape for amorphous configurations. In comparison, annealing the ordinary glass at 296 K (θ_K = 0.09) or 328 K (θ_K = 0.22) is relatively ineffective. Similar results were observed for IMC deposited at T_g – 50 K, with θ_K = 0.23 to 0.44, depending on deposition rate. These results can be put into context by comparison with Kovac's seminal aging experiments on poly(vinylacetate), where 2 months of annealing achieved $\theta_K \leq 0.17$ (*16*).

Vapor deposition can also create unusually dense glasses. The ratio of the density of vapor-deposited TNB (ρ_{VD}) to that of the ordinary glass (ρ_o, prepared by cooling from the liquid) increases as the deposition temperature is lowered toward T_g – 50 K (Fig. 2). Also shown as the solid line is a prediction of the density if vapor deposition produced an equilibrium supercooled liquid at the deposition temperature (*12*). For this range of deposition temperatures, our samples nearly achieve this upper bound for the density. If we define a fictive temperature based on density, deposition at 296 K produces $T_f \approx$ 300 K, slightly lower than the fictive temperature based on the enthalpy (*15*).

We have used neutron reflectivity to characterize diffusion in glasses of TNB. The high spatial resolution and large contrast in the scattering length of neutrons for hydrogen and deuterium nuclei make this an excellent technique for quantifying molecular motion. As schematically shown in the inset of Fig. 3, 300-nm films were prepared by alternately vapor-depositing 30-nm-thick layers of protio TNB (h-TNB) and deuterio TNB (d-TNB) (*17*). The specular reflectivity R was measured as a function of beam angle relative to the sample surface. This value, multiplied by q^4 for clarity, is plotted as a function of the wave vector q. Reflectivity curves for samples vapor-deposited at different temperatures display diffraction peaks; as expected for our symmetric multilayer samples, only odd diffraction orders are present. For samples deposited at low temperature, diffraction can be observed up to the 13th order, indicating very sharp h-TNB/d-TNB interfaces (*15*).

Time series of neutron reflectivity curves were obtained for two vapor-deposited samples during annealing at 342 K for samples deposited at 330 K (Fig. 4A) or 296 K (Fig. 4B). During 8 hours of annealing, all diffraction peaks (except the first-order peak) for sample A decayed to zero, indicating that substantial interfacial broadening had occurred because of interdiffusion of h-TNB/d-TNB. During the 16 hours of annealing at 342 K for sample B, no detectable interdiffusion occurred, even on the single-nanometer length scale. We emphasize that the only difference between these two samples was the temperature at which the substrate was held during deposition.

Figure 4A illustrates the behavior of an ordinary glass annealed near T_g; as shown elsewhere (*17*), interdiffusion in this sample is characteristic of the equilibrium liquid. In contrast, the sample deposited near T_g – 50 K (Fig. 4B) is kinetically much more stable, in qualitative agreement with the high onset temperature shown for the vapor-deposited sample in Fig. 1A. We can quantify the magnitude of this stability in terms of the equilibrium structural relaxation time

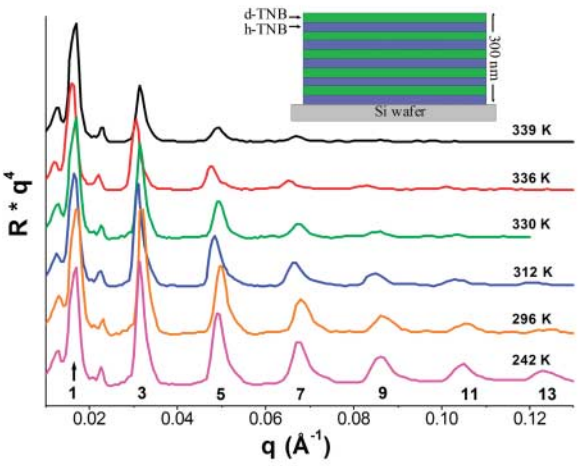

Fig. 3. Neutron reflectivity versus wave vector q for multilayer TNB films vapor-deposited at the specified temperatures. The peak intensities are determined by the sharpness of the h-TNB/d-TNB interfaces, which vary from 1.5 to 9 nm (full width at half maximum of the concentration profile derivative). The diffraction order of each peak is given by the numbers at the bottom. The inset illustrates the structure of the vapor-deposited sample (*15*).

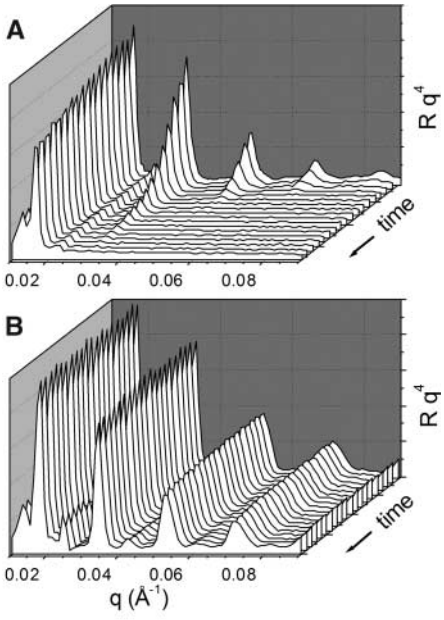

Fig. 4. Neutron reflectivity data for TNB multilayer films continuously annealed at 342 K. The substrate temperature during vapor deposition was (**A**) 330 K and (**B**) 296 K. The decay of the harmonic peaks in (A) occurred over 8 hours and is caused by bulk molecular diffusion (*17*). No detectible diffusion occurred in (B) over 16 hours (*15*).

τ_α, known to be 250 s at 342 K (*18*). The induction time for the sample deposited at $T_g - 50$ K exceeds 200 τ_α. Consistent with this result, we have observed in preliminary experiments that crystal growth rates in stable, vapor-deposited TNB glasses are slower than in ordinary glasses, although the former may contain crystal nuclei.

The reflectivity curves in Fig. 3 provide insight into the mechanism that allows vapor deposition to create unusually stable glasses. The average h-TNB/d-TNB interface widths of the as-deposited samples were extracted from fits to the raw data (*17*) and ranged from 9 nm for the sample deposited at 339 K to 1.5 nm for deposition at 242 K. For all samples deposited at 296 K or above, the interfacial width exceeds the surface roughness (~1.5 nm) as determined by x-ray and neutron reflectivity and the broadening estimated for bulk diffusion during the deposition process (*17*). Deposition at 242 K (T_g – 100 K) produced interfacial widths that are consistent with the surface roughness.

Because the h-TNB/d-TNB interface widths for deposition temperatures above 242 K cannot be explained by surface roughness or bulk diffusion, we tentatively attribute them to enhanced mobility within a few nanometers of the surface of a TNB glass. Such mobility would explain both the broad interfaces observed in the as-deposited samples and the unusually stable glasses formed by vapor deposition. At the deposition rates used in our experiments (0.1 to 5 nm/s), TNB molecules would be a part of the mobile surface layer for ~1 s before they are buried and become part of the bulk glass. If molecules at the surface can substantially rearrange in 1 s, they can find configurations that are near equilibrium configurations at the temperature of the substrate, even if the substrate is well below T_g.

This rapid configuration sampling at the surface would, in a layer-by-layer fashion, produce a bulk glass that is low in the energy landscape with unusually high density and kinetic stability. It would also produce the broad interfaces observed for deposition at temperatures of 296 K and above. Enhanced surface dynamics similar to those in our proposed mechanism have been recently reported. By measuring voltage changes induced by the motions of implanted ions, Cowin and co-workers deduced a marked decrease of the viscosity for the top 3 nm of thin films of supercooled 3-methylpentane (*19*). Numerous studies have found evidence for enhanced mobility at the surface of glassy polymer films (*20*–*23*).

The surface-mobility mechanism for the creation of unusually stable glasses is supported by an order-of-magnitude calculation. TNB samples vapor-deposited at 296 K have interface widths of 2.5 nm, clearly in excess of the width associated with surface roughness. We attribute the additional 1 nm of interface width to surface mobility and, given a deposition rate of 0.1 nm/s, the molecules are within the mobile surface layer for 10 s. Combining this length and time yields an estimate for the surface diffusion coefficient of 5×10^{-16} cm^2/sec. For bulk TNB, this diffusion coefficient is found near T_g, where the structural relaxation time τ_α is a few seconds (*17*, *18*). Thus, surface molecules plausibly remain mobile for several structural relaxation times before becoming buried, arguably long enough to find near-equilibrium configurations at 296 K.

Given the widespread use of vapor-deposition techniques, it is surprising that unusually stable glasses have not been reported previously. In fact, it is commonly reported that vapor-deposition creates low-density glasses with low kinetic and thermodynamic stability (*24*–*26*). As compared with many reported depositions of metallic and organic materials, we have used lower deposition rates and/or substrate temperatures that are nearer to T_g. We observe the creation of highly stable glasses only for substrate temperatures T_{dep}/T_g in the vicinity of 0.85. Additionally, we observe that increasing the deposition rate can considerably decrease the stability of the glasses formed. These observations are all consistent with our proposed mechanism: Faster deposition does not allow as much time for equilibration at the surface and, at low enough temperature, surface molecules will rearrange too slowly to equilibrate. Indeed, the metallic glass community has known for decades that fast, low-temperature deposition is required to prepare high-energy glasses that quench thermodynamically unstable mixtures (*27*).

We speculate that unusually stable glasses can be prepared for many systems that can be vapor-deposited, if surface mobility is enhanced and the substrate temperature is appropriately controlled. We anticipate that the availability of low-energy glasses prepared by vapor deposition and less general routes (*28*) will allow new insights into glass formation and the nature of the lower regions of the energy landscape. Stable glasses could also affect technologies such as amorphous pharmaceuticals, where stability against crystallization is required to retain the enhanced bioavailability of amorphous preparation.

References and Notes

1. C. A. Angell, *J. Res. Natl. Inst. Stand. Technol.* **102**, 171 (1997).
2. P. G. Debenedetti, F. H. Stillinger, *Nature* **410**, 259 (2001).
3. F. H. Stillinger, *Science* **267**, 1935 (1995).
4. M. D. Ediger, C. A. Angell, S. R. Nagel, *J. Phys. Chem.* **100**, 13200 (1996).
5. W. Kauzmann, *Chem. Rev.* **43**, 219 (1948).
6. F. H. Stillinger, *J. Chem. Phys.* **88**, 7818 (1988).
7. R. J. Speedy, *Biophys. Chem.* **105**, 411 (2003).
8. A. Saksaengwijit, J. Reinisch, A. Heuer, *Phys. Rev. Lett.* **93**, 235701 (2004).

9. H. Tanaka, *Phys. Rev. E* **68**, 011505 (2003).
10. D. H. Huang, S. L. Simon, G. B. McKenna, *J. Chem. Phys.* **119**, 3590 (2003).
11. D. V. Matyushov, C. A. Angell, *J. Chem. Phys.* **123**, 034506 (2005).
12. D. J. Plazek, J. H. Magill, *J. Chem. Phys.* **45**, 3038 (1966).
13. C. M. Whitaker, R. J. McMahon, *J. Phys. Chem.* **100**, 1081 (1996).
14. J. H. Magill, *J. Chem. Phys.* **47**, 2802 (1967).
15. Materials and methods are available as supporting material on *Science* Online.
16. A. J. Kovacs, *Fortschr. Hochpolym-Forsch.* **3**, 394 (1963).
17. S. F. Swallen *et al.*, *J. Chem. Phys.* **124**, 184501 (2006).
18. R. Richert, K. Duvvuri, L.-T. Duong, *J. Chem. Phys.* **118**, 1828 (2003).
19. R. C. Bell, H. F. Wang, M. J. Iedema, J. P. Cowin, *J. Am. Chem. Soc.* **125**, 5176 (2003).
20. C. J. Ellison, J. M. Torkelson, *Nat. Mater.* **2**, 695 (2003).
21. S. Kawana, R. A. L. Jones, *Phys. Rev. E* **63**, 021501 (2001).
22. J. L. Keddie, R. A. L. Jones, R. A. Cory, *Faraday Discuss.* **98**, 219 (1994).
23. J. A. Forrest, K. Dalnoki-Veress, J. R. Stevens, J. R. Dutcher, *Phys. Rev. Lett.* **77**, 2002 (1996).
24. F. Faupel *et al.*, *Rev. Mod. Phys.* **75**, 237 (2003).
25. K. Ishii, H. Nakayama, T. Okamura, M. Yamamoto, T. Hosokawa, *J. Phys. Chem. B* **107**, 876 (2003).
26. K. Takeda, O. Yamamuro, H. Suga, *J. Phys. Chem.* **99**, 1602 (1995).
27. D. Turnbull, *Metall. Mater. Trans. A* **12**, 695 (1981).
28. H. Tanaka, R. Kurita, H. Mataki, *Phys. Rev. Lett.* **92**, 025701 (2004).

29. We acknowledge support for this work from NSF CHE-0605136, NSF-0412707, and USDA 2005-01303.

Supporting Online Material

www.sciencemag.org/cgi/content/full/1135795/DC1
Materials and Methods
Fig. S1
References

2 October 2006; accepted 27 November 2006
Published online 7 December 2006;
10.1126/science.1135795
Include this information when citing this paper.

Unexpected Stability of Al_4H_6: A Borane Analog?

X. Li,[1] A. Grubisic,[1] S. T. Stokes,[1] J. Cordes,[1,2] G. F. Ganteför,[1,2] K. H. Bowen,[1]* B. Kiran,[3] M. Willis,[3] P. Jena,[3] R. Burgert,[4] H. Schnöckel[4]

Whereas boron has many hydrides, aluminum has been thought to exhibit relatively few. A combined anion photoelectron and density functional theory computational study of the $Al_4H_6^-$ anion and its corresponding neutral, Al_4H_6, showed that Al_4H_6 can be understood in terms of the Wade-Mingos rules for electron counting, suggesting that it may be a borane analog. The data support an Al_4H_6 structure with a distorted tetrahedral aluminum atom framework, four terminal Al-H bonds, and two sets of counter-positioned Al-H-Al bridging bonds. The large gap between the highest occupied and the lowest unoccupied molecular orbitals found for Al_4H_6, together with its exceptionally high heat of combustion, further suggests that Al_4H_6 may be an important energetic material if it can be prepared in bulk.

Even though aluminum and boron are sister elements in the periodic table, aluminum forms only a few hydrides, whereas boron has many, known as the boranes. The known hydride chemistry of aluminum is limited to AlH_3 and Al_2H_6, seen in cryogenic matrices (*1*, *2*) and perhaps the gas phase (*3*); alane, $(AlH_3)_n$, a polymeric solid; AlH_4^- and its alkali metal salts, the alanates, such as $LiAlH_4$ (*4*); $Al_{13}H^-$ formed in beams (*5*, *6*); and dissociative chemisorption products of $D_2 + Al_n^-$ interactions in beams (*7*). Boron hydrides, in contrast, exhibit a broad diversity of stoichiometries, such as B_2H_6, B_4H_{10}, B_5H_9, B_6H_{10}, and $B_{10}H_{14}$ (*8*–*11*). Given the electronic similarity between aluminum and boron, the lack of a comparable aluminum hydride chemistry is puzzling. Are analogous aluminum hydrides simply unstable under all circumstances, or might there be pathways by which they can be formed and environments in which they are stable?

We explored these questions by rapidly vaporizing aluminum metal in the presence of an abundant, albeit momentary, concentration of hydrogen atoms and the cooling environment of a fast helium gas expansion. These conditions were provided by a pulsed arc discharge source (PACIS) (*5*, *12*). The value of the PACIS source for studying aluminum cluster anion and hydrogen interactions was first realized by Ganteför and co-workers, who used it in photoelectron studies of HAl_{13}^- and similarly sized aluminum cluster anions, each with up to two hydrogen atoms attached (*5*). In our study, such a source provided a doorway into a much wider world of aluminum hydride cluster anions. In a PACIS source, a discharge is struck between an anode and a grounded, metallic sample cathode as helium gas from a pulsed valve flows through the discharge region (Fig. 1). When an extender tube is added to this arrangement, additional gases can be added downstream. In our study, the sample electrode was aluminum, and hydrogen gas was back-filled before each discharge event. Upon initiation of the pulsed discharge, a plasma containing hydrogen atoms (the latter formed by the dissociation of H_2) expanded down the extender tube, cooling, clustering, and reacting along the way. The resulting anions were then subjected to extraction and mass analysis by a time-of-flight mass spectrometer. Their mass spectra revealed that between 1 and 10 hydrogen atoms had been attached to each aluminum cluster anion size. A typical experiment in which aluminum cluster anions, Al_n^- (n = 3 to 20), were generated thus revealed roughly 200 previously unobserved aluminum hydride anions. A por-

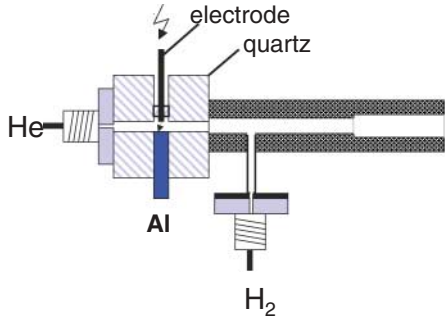

Fig. 1. Schematic diagram of a PACIS source.

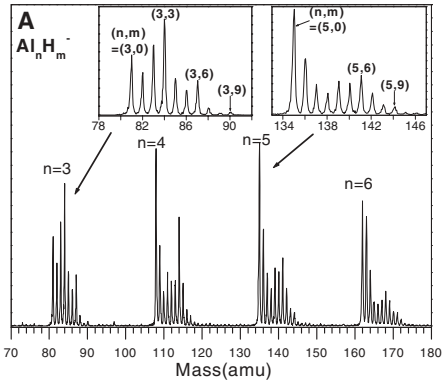

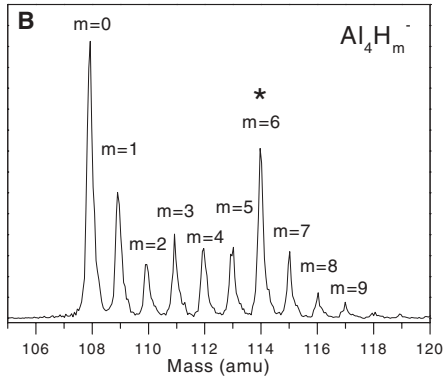

Fig. 2. (**A**) Mass spectrum showing the wide variety of $Al_nH_m^-$ anions that are formed with the PACIS source. Insets show magnified views of selected portions of the mass spectrum, revealing individual $AL_nH_m^-$ species. (**B**) A portion of the mass spectrum showing only the $Al_4H_m^-$ series.

[1]Departments of Chemistry and Materials Science, Johns Hopkins University, Baltimore, MD 21218, USA. [2]Department of Physics, University of Konstanz, 78457 Konstanz, Germany. [3]Department of Physics, Virginia Commonwealth University, Richmond, VA 23284, USA. [4]Institute of Inorganic Chemistry, University of Karlsruhe (TH), 76128 Karlsruhe, Germany.

*To whom correspondence should be addressed. E-mail: kbowen@jhu.edu